

A piecewise constant levelset approach for semi-blind deconvolution: Application to barcode decoding

A. De Cezaro[†] E. Hafemann^{‡§} A. Leitão[‡]

June 2, 2026

Abstract

We consider a semi-blind deconvolution problem arising in the decoding of blurred linear barcodes. Building on the Piecewise Constant Level Set (PCLS) framework introduced in [De Cezaro et al., *Inv. Probl.*, 29 (2013), 015003], we propose and analyze a solution method based on augmented Lagrangians to obtain stable approximate solutions to the corresponding inverse problem with respect to noisy measurements. We establish the existence of generalized multipliers for the augmented Lagrangian functional under consideration, as well as the absence of duality gaps. These results provide the theoretical foundation required to prove regularization properties of the approximate solutions produced by the proposed strategy. Furthermore, we present an associated ADMM-type iterative scheme for the explicit computation of approximate barcodes. Numerical experiments are carried out for various variance values (responsible for the blurred effect) and several levels of noise, validating the effectiveness of the proposed method.

Keywords. Semi-blind deconvolution, Barcode decoding, Piecewise constant levelset, Augmented Lagrangian .

AMS Classification: 65J20, 47J06, 65R32.

1 Introduction

A *barcode* (or bar code) image serves as a visual representation of data. A linear (or 1D) barcode, for example, comprises parallel lines and bars with differing widths and gaps, encoding specific information. Different barcode symbologies do exist, each with its unique pattern for encoding data, e.g., linear type codes (e.g., ISBN, MSI, Royal Mail-4, 2-of-5 IATA, UPC and Code-128) and 2D type codes (including QR-Code, Data Matrix, PDF417, MaxiCode and Aztec); visit the TEC-IT website <https://www.tec-it.com/> for a detailed presentation on barcode symbologies.

Barcode decoding: Barcodes find extensive application across diverse industries, serving multiple purposes, e.g., inventory management, retail sales, tracking shipments and ticketing. When scanned, a linear barcode pattern of bars and spaces is translated into alphanumeric characters, allowing the encoded information to be utilized. The swift and precise scanning by barcode readers plays a crucial role in the application of this technology.

[†]Institute of Math. Statistics and Physics, Federal Univ. of Rio Grande, Av. Italia km 8, 96201-900 Rio Grande, Brazil

[‡]Department of Mathematics, Federal University of St. Catarina, P.O. Box 476, 88040-900 Floripa, Brazil

[§]Fachbereich Mathematik, Universität Hamburg, Bundesstraße 55, 20146 Hamburg, Germany

Emails: decezarontm@gmail.com, eduardo.hafemann@uni-hamburg.de, acgleitao@gmail.com.

The decoding of the information in a linear barcode is typically due to an optical scanner equipped with a light detector. A narrow laser beam is emitted, which illuminates the barcode –Figure 1 (right). The amount of light detected, namely a voltage reading, generates a 1D electrical signal with peaks corresponding to the white parts (due high light reflection) and valleys corresponding to the black bars (due to little light reflection); see Figure 1 (left).

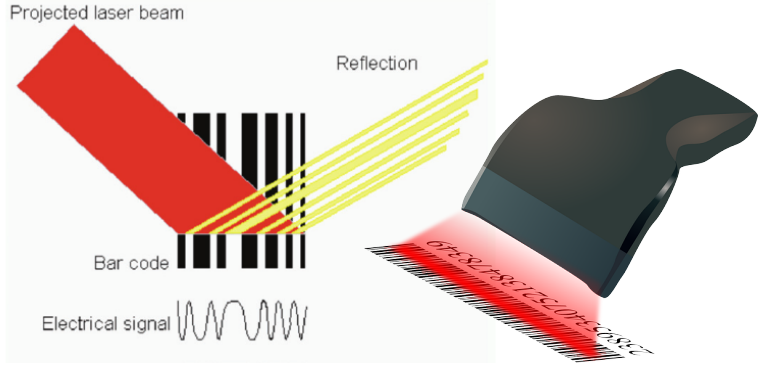


Figure 1: Barcode optical scanner (source: pixabay.com).

Mathematical model: In this 1D setup the barcode can be described as a piecewise constant function u taking only two different known values (namely, zero for black and one for white) in a given connected bounded interval $\Omega \subset \mathbb{R}$. More precisely, we assume the existence of an open measurable set $D_1 \subset \subset \Omega$ such that

$$u(x) = 0, \quad x \in D_1 \quad \text{and} \quad u(x) = 1, \quad x \in D_2 := \Omega \setminus D_1. \quad (1)$$

The laser beam has a variable intensity profile of a finite width. Consequently, the voltage readings of the barcode by the scanner (available measurements) suffer non-local effects. Since the black bars in the barcode u are finite (Ω is bounded), the non-local effects far from the barcode location do not influence the scanning process. Hence, in the mathematical model considered in this article, we assume that the effects of the laser beam on the barcode are modeled by a point-spread function (PSF) with compact support

$$K(x) = K(\gamma, \sigma)(x) = \chi_{\Omega}(x) \frac{\gamma}{\sigma\sqrt{2\pi}} e^{-\frac{x^2}{2\sigma^2}}, \quad (2)$$

where the variance σ^2 models the distance between the scanner and the bar code surface (the longer the distance from the scanner to the barcode, the larger the variance) and $\gamma > 0$ is the amplitude of the Gaussian kernel K (γ encapsulates the process of converting light energy that interacts with the barcode into the measurement). Additionally, χ_{Ω} denotes the characteristic function of Ω . Since the coefficients (σ, γ) are not known, the kernel K in (2) is only partially known.

We consider the setting in which the amplitude γ of the kernel K is known. The inverse problem under investigation consists of identifying both the variance σ^2 and the barcode u .

The interaction of the barcode with the laser beam is modeled by the nonlinear operator

$$\begin{aligned} B : L^2(\Omega) \times L^1(\Omega) &\longrightarrow L^2(\Omega) \\ (K, u) &\longmapsto B(K, u) := K * u, \end{aligned} \quad (3)$$

where the symbol $*$ represents the convolution operation; the functions $u \in L^1(\Omega)$ and $K \in L^2(\Omega)$ are given as above. The signal (or sensor reading) $y \in L^2(\Omega)$ resulting from this interaction is described by the well established mathematical model $y = K * u$ (see, e.g., [14, 15]).

Underlying inverse problem: The transformation of the barcode into the signal that is actually detected by the scanner depends on a variety of factors such as: distance between the optical scanner and the surface where the barcode appears (the farther away the scanner is located, the more distorted/blurred the detected signal), the illumination of the optical sensor (inside the barcode scanner), among others. Therefore, in practice, only a noise version $y^\delta \in L^2(\Omega)$ of the signal y is available. We assume that the level of noise δ in the signal can be estimated by

$$\|y - y^\delta\|_{L^2(\Omega)} \leq \delta. \quad (4)$$

Summarizing, the inverse problem we are dealing with is the one of identifying the pair (K, u) in the operator equation

$$B(K, u) = y^\delta, \quad (5)$$

from noise measurements y^δ of the signal y satisfying (4). An efficient method designed for solving (5), (4) should take into account the following *a priori* information: (i) available partial knowledge of the PSF K , which is known to be of the form (2); (ii) the fact that u (the barcode) is a piecewise constant function satisfying (1).

The barcode identification problem considered here differs from the standard image analysis problems of image deblurring [3, 15] and blind deconvolution [31, 22, 26]. Here the convolution kernel K is not completely known and the scalar parameter σ must be identified together with the barcode u . In other words, this linear barcode identification problem can be viewed as a *semi-blind deconvolution problem* [14, 6, 21].

Literature overview: There is a vast amount of literature on barcode decoding. In this paragraph, we focus on some inverse problems (and imaging) approaches that are relevant to the content covered in this manuscript.

Commercial deblurring techniques for hand scanners are often based on edge detection, which plays a relevant role in barcode decoding. These techniques relate to the search for local extrema of the derivative of the noisy signal y^δ (zero crossings of the second derivative provide edge features for the classification of blurred images); however, it is known to be highly sensitive to small changes in the data (ill-posedness) [13]. Another drawback of this strategy is related to the standard deviation σ . If σ is "large" or if the support size of K is very large when compared to the smallest length scale of the minimum thickness of bars in the barcode, then the extremes of the derivative of y^δ might not correspond to the edges of the barcode to be decoded, even when $\delta = 0$. In [20] the edge localization error caused by speckle noise (e.g., when a barcode signal is corrupted by additive noise which is a weakly stationary random process) is estimated. In [19] the severely blurred image scenario is considered; statistical pattern recognition is used to classify the peaks as (UPC) barcode characters.

In [14] the semi-blind decoding of linear barcodes in (5), with K as in (2), is considered. Energy minimization strategies with total-variation (TV) penalization are proposed and analyzed for the stable barcode decoding problem (5) with noise measurements y^δ (e.g., existence and uniqueness of minimizers (γ, σ, u) for a Tikhonov functional based on TV-penalization is proven in [14, Proposition 4]). The recovered barcode is numerically obtained as the Γ limit of a "diffuse interface" approximation of an energy minimization strategy, with a distinct level of blurring σ .

Other approaches to semi-blind barcode decoding are considered in [21, 26]. In [21], for 1D barcodes, the authors investigate the effect of nonstationary out-of-focus blurring, i.e. when $(\gamma, \sigma) = (\gamma(s), \sigma(s))$ (s is used to parameterize the depth map of the barcode by its arc length [21, Figure 1]). An algorithm based on the minimization of an energy functional (using penalization that includes the l_0 gradient norm of u) is proposed. A low-dimensional representation of the PSF is estimated using the Levenberg–Marquardt method. Once the PSF is obtained, a deblurred image is computed by solving a quadratic program (a $[0, 1]$ box constraint is used to enforce a binary signal). In [26] a penalization based on Kullback-Leibler divergence is considered for semi-blind decoding of UPC-A and QR barcodes. The proposed approach, which incorporates and exploits barcode symbologies, uses a primal-dual strategy. The method does not aim to directly locate the cleaned image; instead, it determines the probability density function of the image across all binary arrays. Subsequently, the cleaned image is derived from its threshold expectation.

In [15] a deblurring problem related to (5) is considered. The blur kernel K is assumed to be known. The authors provide conditions, depending on σ and the additive noise level, under which the variational method proposed in [14] is able to recover the barcode. The analysis in [15] is extended in [28] for camera-reading decoding of UPC barcodes, where the authors prove that, if

the UPC barcode has the narrowest bar corresponding to two thirds the size of the camera pixel, the encoded message in the barcode can be uniquely determined.

In [18] a symbology-based reconstruction of the UPC barcode decoding problem is investigated. The symbology of the barcode is incorporated directly into the reconstruction algorithm and a sparse representation of the barcode is reconstructed with respect to this dictionary (this approach reduces the number of degrees of freedom in the problem).

In [9] total variation-based energy penalization is used to recover a blurred 1D barcode. Tikhonov functionals defined over all possible barcodes with fidelity to a convoluted signal of a barcode and regularized by a BV -term. The fidelity terms consist of the L^2 -distance to the measured signal (or preceded by deconvolution). The authors established sufficient conditions for the support of K , the level of blurring σ , the size of the bars and the regularization parameters where the underlying bar code is the unique minimizer. In [10] the same authors apply total variation penalization and L^1 -fidelity to the recovery of blurred 2D barcodes.

Main contributions: We introduce and study a regularization technique that relies on the primal solutions of a special augmented Lagrangian functional linked to the underlying inverse problem. Specifically, we establish the existence of generalized multipliers for the augmented Lagrangian functional under study and show that no duality gap occurs. These findings form the theoretical basis needed to prove the regularization behavior of the approximate solutions generated by the proposed approach.

We also provide an ADMM-type iterative algorithm for the explicit computation of approximate barcodes. Numerical experiments are conducted for a range of variance parameters (governing the blurring effects) and noise intensities, confirming the effectiveness of the proposed method.

2 PCLS ansatz, slack variable, augmented Lagrangian

In this section we discuss three important tools for computing stable approximate solutions $(K_\alpha^\delta, \phi_\alpha^\delta)$ to the inverse problem (4), (5), namely: 1) A PCLS ansatz (6) used to represent the unknown barcode; 2) the introduction of a slack variable regarding K (this is a quintessential step that enables the use of augmented Lagrangians); 3) An augmented Lagrangian functional (11) that allows the effective computation of the desired approximate solutions.

Piecewise Constant Level-Sets: In [12] a PCLS ansatz is used to represent the solution of a nonlinear ill-posed operator equation, under the *a priori* assumption that the sought solution is a piecewise constant function taking only two possible (unknown) values [30, 24, 11, 12, 2]. According to this approach, a function $u \in \text{BV}(\Omega)$ satisfying $u(x) \in \{c^1, c^2\}$ a.e. in Ω is represented by

$$u = c^1 \psi_1(\hat{\phi}) + c^2 \psi_2(\hat{\phi}) =: P_{pc}(\hat{\phi}), \quad (6)$$

where $\hat{\phi} : \Omega \rightarrow \mathbb{R}$ is the piecewise constant levelset function defined by $\hat{\phi}(x) := i - 1$, $x \in D_i$, for $i = 1, 2$, and $\psi_1(t) = 1 - t$, $\psi_2(t) = t$ are real functions.

Remark 1. *In the setting discussed in Section 1 the function u represents the unknown barcode, which is known to satisfy $u(x) \in \{0, 1\}$ a.e. in Ω (see [14, 31, 10]). This is equivalent to choosing $c^1 = 0$ and $c^2 = 1$ in (6). With this particular choice, the operator P_{pc} in (6) reduces to the identity operator.*

Here the PCLS ansatz (6) is used to represent the component u of the solution pair (K, u) of the inverse problem (5), (4). This allow us to incorporate to the operator equation (5) the *a priori* information described in (1). In view of Remark 1, the inverse problem of barcode decoding becomes the one of identifying the pair (K, ϕ) in the system

$$\begin{cases} B(K, \phi) = y^\delta \\ \mathcal{W}(\phi) = 0 \end{cases}, \quad (7)$$

from noise measurements y^δ satisfying (4). Here K has the same meaning as in (5) and $\phi \in L^{4n}(\Omega) \cap \text{BV}(\Omega)$ is a Piecewise Constant LevelSet function. Additionally, $\mathcal{W} : L^{4n}(\Omega) \cap \text{BV}(\Omega) \rightarrow L^2(\Omega)$ is the nonlinear double-well operator defined by $\mathcal{W}(\phi) := \phi^n(\phi - 1)^n$, for $n \in \{1, 2, \dots\}$ (see, e.g., [30, 24] for details).

Remark 2. Notice that the level set function $\hat{\phi} \in L^{4n}(\Omega) \cap \text{BV}(\Omega)$ in (6) satisfies $\hat{\phi}(x) := i - 1$, $x \in D_i$, $i = 1, 2$; therefore $\mathcal{W}(\hat{\phi}) = 0$. On the other hand, if $\mathcal{W}(\phi) = 0$ for some function $\phi \in L^{4n}(\Omega) \cap \text{BV}(\Omega)$ then $\phi(x) \in \{0, 1\}$, a.e. in Ω (see Lemma 7 (ii) below). Consequently, any solution (K, ϕ) of system (7) is also a solution of (5) having piecewise constant component ϕ .

In order to obtain stable approximate solutions to problem (7), (4) we consider the minimizers $(K_\alpha^\delta, \phi_\alpha^\delta)$, if exist, of the (regularized) constrained optimization problem

$$\begin{cases} \min F_\alpha(K, \phi) := \|B(K, \phi) - y^\delta\|_{L^2(\Omega)}^2 + \alpha R(K, \phi) \\ \text{s.t. } \mathcal{W}(\phi) = 0 \end{cases}, \quad (8)$$

where $F_\alpha : L^2(\Omega) \times (L^{4n}(\Omega) \cap \text{BV}(\Omega)) \rightarrow \mathbb{R}_+$ and the penalization functional $R : L^2(\Omega) \times (L^{4n}(\Omega) \cap \text{BV}(\Omega)) \rightarrow \mathbb{R}_+$ is defined by

$$R(K, \phi) := \beta_1 \|K - K_0\|_{H^1(\Omega)}^2 + \beta_2 \|\phi\|_{L^{4n}}^2 + \beta_3 |\phi|_{\text{BV}}. \quad (9)$$

Here $K_0 \in H^1(\Omega)$ is some *a priori* and $\beta_j > 0$ for $j = 1, 2, 3$ are scaling factors. Furthermore, $\alpha > 0$ plays the role of a regularization parameter as in classical Tikhonov regularization [13].

Remark 3. In view of the continuity of the bilinear operator $B(\cdot, \cdot)$, see Proposition 9, the existence of $(K_\alpha^\delta, \phi_\alpha^\delta) = \text{argmin } F_\alpha(K, \phi)$, follows from standard compactness arguments [13]. However, there is no guarantee that ϕ_α^δ satisfies the desired constraint $\mathcal{W}(\phi_\alpha^\delta) = 0$. Notice that this constraint cannot be enforced by standard projection strategies, since the levelset $\{\phi \in L^{4n}(\Omega), : \mathcal{W}(\phi) = 0\}$ is not a convex subset of $L^{4n}(\Omega)$.

A well established technique in the optimization literature [4, 27] is to solve the constraint optimization problem (8) is by means of duality theory (also known as the Lagrangian approach). In the case where K is known, i.e. the deblurring problem, a regularization approach based on the augmented Lagrangian formulation for problem (8) is possible (following the lines of the analysis presented in Section 3). In particular, the existence of a generalized Lagrangian multiplier λ_K supporting an exact penalty (in this case $\mathcal{W}(\phi) = 0$) follows, with the necessary adaptations, similarly to the one presented below in Subsection 3.1. However, the K -dependence of such a Lagrangian multiplier λ_K makes the ongoing theory intractable, as far as we know, if K is also unknown.

Introduction of a slack variable: Notice that to each solution $(K_\alpha^\delta, \phi_\alpha^\delta)$ of (8), there corresponds a solution of the optimization problem

$$\begin{cases} \min \mathcal{F}_\alpha(\mathcal{K}, K, \phi) := \|B(K, \phi) - y^\delta\|_{L^2(\Omega)}^2 + \alpha \mathcal{R}(\mathcal{K}, K, \phi) \\ \text{s.t. } \mathcal{W}(\phi) = 0 \text{ and } M(\mathcal{K}, K) = 0 \end{cases}, \quad (10)$$

where the functionals \mathcal{F}_α and \mathcal{R} map from $X := L^2(\Omega) \times L^2(\Omega) \times (L^{4n}(\Omega) \cap \text{BV}(\Omega))$ to \mathbb{R}_+ , with $\mathcal{R}(\mathcal{K}, K, \phi) := R(K, \phi) + \beta_1 \|\mathcal{K} - K_0\|_{H^1(\Omega)}$. Moreover, $M : L^2(\Omega) \times L^2(\Omega) \rightarrow L^2(\Omega)$ is defined by $M(\mathcal{K}, K) := \mathcal{K} - K$ and \mathcal{W} is defined as in (7).

In problem (10) the slack variable \mathcal{K} is introduced (in [6] a similar technique is used for semi-blind regularization). This strategy is known from the Alternation Direction Method of Multipliers (ADMM) [6] and from the equality/inequality constraint optimization theory [4, 27]. It has the disadvantage of increasing the number of unknowns (when compared to (8)). However, the formulation in (10) has the advantage of incorporating equality constraints in all problem unknowns (\mathcal{K}, K, ϕ) . This characteristic is quintessential in the derivation of a complete convergence analysis for the regularization method based on the minimizers of (10) (see Remark 3 and Section 3 for details).

Introduction of augmented Lagrangians: The duality theory followed in this manuscript starts with the introduction of the augmented Lagrangian functional

$$L_\alpha(\mathcal{K}, K, \phi; \lambda, \mu) := \|B(K, \phi) - y^\delta\|_{L^2(\Omega)}^2 + \alpha\mathcal{R}(\mathcal{K}, K, \phi) + \langle \lambda, (M(\mathcal{K}, K), \mathcal{W}(\phi)) \rangle + \mu\|(M(\mathcal{K}, K), \mathcal{W}(\phi))\| \quad (11)$$

(the notation $\langle \cdot, \cdot \rangle$ and $\|\cdot\|$ denote the inner product and norm in $L^2(\Omega) \times L^2(\Omega)$ respectively). Here the primal variables are $(\mathcal{K}, K, \phi) \in X$; the dual variables $(\lambda, \mu) \in (L^2(\Omega))^2 \times \mathbb{R}_+$ are such that: λ can be interpreted as a “generalized Lagrange multiplier” and μ is a penalty factor that allows one to establish a duality relation for problems of non-convex type. This particular augmented Lagrangian functional is also known as the sharp Lagrangian [27, Chapter 11, Section K*].

The Lagrangian functional in (11) converts the (primal) constrained optimization problem (10) into a family of unconstrained sub-problems (depending on $(\lambda, \mu) \in (L^2(\Omega))^2 \times \mathbb{R}_+$), so that the information provided by the constraints $\mathcal{W}(\phi) = 0$ and $M(\mathcal{K}, K) = 0$ is incorporated in the Lagrangian L_α . This approach is effective when the subproblems are simpler to solve than the original constrained problem and the Lagrangian function is able to provide the zero duality gap property (see Subsection 3.1). Since $\mathcal{W}(\phi)$ is nonlinear, the zero duality gap for the constrained optimization problem (10) does not follow straightforward (see Subsection 3.1).

The idea here is to compute regularized solutions $(K_\alpha^\delta, \phi_\alpha^\delta)$, as the minimizer (primal solutions $(\mathcal{K}_\alpha^\delta, K_\alpha^\delta, \phi_\alpha^\delta)$, with $\mathcal{W}(\phi_\alpha^\delta) = 0$ and $M(\mathcal{K}_\alpha^\delta, K_\alpha^\delta) = 0$, of the augmented Lagrangian (11) associated to the constrained optimization problem (10).

3 Convergence analysis

We denote by $Ad \subset X$ the set of admissible functions defined by $Ad := \{(\mathcal{K}, K, \phi) \in X\}$, subject to $\mathcal{W}(\phi) = 0$, $M(\mathcal{K}, K) = 0$ and $K * \phi \in L^2(\Omega)$. In the following, we present the main assumptions used in these notes.

(A1) $\Omega \subseteq \mathbb{R}$, is bounded.

(A2) α, β_j denote positive parameters.

(A3) There exists $\hat{\sigma} > 0$, $\hat{K} = K(\hat{\sigma}) \in L^2(\Omega)$ and $\hat{u} \in \text{BV}(\Omega) \cap L^\infty(\Omega)$ satisfying $B(\hat{K}, \hat{u}) = y$. Moreover, there exists a function $\hat{\phi} \in \text{BV}(\Omega) \cap L^{4n}(\Omega)$ such that $\hat{\phi} = \hat{u}$ and $\mathcal{W}(\hat{\phi}) = 0$.

3.1 Existence of an exact penalty representation

The Tikhonov functional \mathcal{F}_α is not convex, so the classical Lagrange multiplier methods [27] cannot be used to solve (10). This is because it is uncertain whether a zero duality gap property can be established for nonconvex optimization problems [27].

In this subsection, we follow similar ideas presented in [2, 12] to prove the existence of an exact penalty representation (see Definition 2) based on the abstract convexity framework introduced in [27]. It turns out that this property implies the zero-duality gap. Furthermore, it becomes the key ingredient to prove the well-posedness, the convergence, and stability of approximate solutions given by the augmented Lagrangian (11) (see Section 3.2).

We introduce some notation and functions related to the augmented Lagrangian approach that are necessary for the upcoming analysis.

Definition 1. Let \mathcal{F}_α , \mathcal{W} and M be defined in the (10) and the Assumptions **A1** - **A3** holds true.

1. $\Gamma : (L^2(\Omega))^2 \rightrightarrows L^2(\Omega)$ is the function with set values that satisfies $\Gamma(z) := \{(\mathcal{K}, K, \phi) \in X : (M(\mathcal{K}, K), \mathcal{W}(\phi)) = z\}$, for each $z \in (L^2(\Omega))^2$.

2. The indicator function of a set A is defined by $\delta_A(\eta) := 0$, if $\eta \in A$ and $\delta_A(\eta) := +\infty$, otherwise.
3. We define $\widetilde{\mathcal{F}}_\alpha(\mathcal{K}, K, \phi) := \mathcal{F}_\alpha(\mathcal{K}, K, \phi)$, if $(\mathcal{K}, K, \phi) \in X \cap \Gamma(0)$ and $\widetilde{\mathcal{F}}_\alpha(\mathcal{K}, K, \phi) := +\infty$, otherwise.
4. A dualizing parametrization function for $\widetilde{\mathcal{F}}_\alpha$ is chosen in the following way $f : X \times (L^2(\Omega))^2 \rightarrow \mathbb{R} \cup \{+\infty\}$, with $f(\mathcal{K}, K, \phi, z) := \mathcal{F}_\alpha(\mathcal{K}, K, \phi) + \delta_{\Gamma(z)}(\mathcal{K}, K, \phi)$ if $(\mathcal{K}, K, \phi) \in X$ and $f(\mathcal{K}, K, \phi, z) = +\infty$, otherwise. The function f satisfies $f(\mathcal{K}, K, \phi, 0) = \widetilde{\mathcal{F}}_\alpha(\mathcal{K}, K, \phi)$, for each $(\mathcal{K}, K, \phi) \in X$.
5. The perturbation function (of the primal problem) related to this duality parametrization is given by $\theta : (L^2(\Omega))^2 \rightarrow \mathbb{R}$, where $\theta(z) := \inf_{(\mathcal{K}, K, \phi) \in X} f(\mathcal{K}, K, \phi, z)$.
6. The coupling function $\rho : (L^2(\Omega))^2 \times (L^2(\Omega))^2 \times \mathbb{R}_+ \rightarrow \mathbb{R}$ is defined by $\rho(z, \lambda, \mu) := -\langle \lambda, z \rangle - \mu \|z\|$.
7. The augmented Lagrangian functional induced by the coupling function ρ reads as

$$\mathcal{L}_\alpha(\mathcal{K}, K, \phi; \lambda, \mu) = \inf_{z \in (L^2(\Omega))^2} \{f(\mathcal{K}, K, \phi, z) - \rho(z, \lambda, \mu)\}. \quad (12)$$

8. The dual function $Q : (L^2(\Omega))^2 \times \mathbb{R}_+ \rightarrow \mathbb{R}$ is defined by

$$Q(\lambda, \mu) := \inf_{(\mathcal{K}, K, \phi) \in X} \mathcal{L}_\alpha(\mathcal{K}, K, \phi; \lambda, \mu)$$

and the dual problem is stated as

$$\text{maximize } Q(\lambda, \mu) \quad \text{subject to } (\lambda, \mu) \in (L^2(\Omega))^2 \times \mathbb{R}_+.$$

It follows from item 5 of Definition 1 that L_α defined in (11) coincides with \mathcal{L}_α in (12), for any $(\mathcal{K}, K, \phi) \in \Gamma(z)$ (indeed, the dualizing parameter function f satisfies $f(\mathcal{K}, K, \phi, z) = +\infty$ whenever $(\mathcal{K}, K, \phi) \notin \Gamma(z)$).

Notice that $\mathcal{L}_\alpha(\mathcal{K}, K, \phi; \lambda, \mu)$ coincides with $\mathcal{F}_\alpha(\mathcal{K}, K, \phi)$ in (10), whenever $\mathcal{W}(\phi) = 0$ and $M(\mathcal{K}, K) = 0$ (indeed, $\mathcal{W}(\phi) = 0$ and $M(\mathcal{K}, K) = 0$ imply $(\mathcal{K}, K, \phi) \in \Gamma(0)$).

From item 8 of Definition 1, it can be deduced that $Q(\lambda, \mu)$ is equal to the infimum of $\theta(z) - \rho(z, \lambda, \mu)$ over all z in $(L^2(\Omega))^2$, with θ being the perturbation function and ρ the coupling function (see items 5 and 6).

Let $V_p := \inf_{(\mathcal{K}, K, \phi) \in X} \widetilde{\mathcal{F}}_\alpha(\mathcal{K}, K, \phi)$ and $V_d := \sup_{(\lambda, \mu) \in (L^2(\Omega))^2 \times \mathbb{R}_+} Q(\lambda, \mu)$ be the optimal values of the primal and dual problems respectively. It follows from the definitions of f and ρ that our scheme has the weak duality property, i.e.

$$V_d \leq V_p. \quad (13)$$

The difference between the values of V_p and V_d is known as the duality gap. The upcoming analysis of the augmented Lagrangian approach requires an exact penalty representation [7, 27] as its primary element, as it implies a zero duality gap, as shown in the following.

Definition 2. A vector $\bar{\lambda} \in (L^2(\Omega))^2$ is said to support an exact penalty representation for the problem of minimizing $\widetilde{\mathcal{F}}_\alpha$, if there exists $\bar{\mu} > 0$ such that for any $\mu > \bar{\mu}$

$$\theta(0) = Q(\bar{\lambda}, \mu) \quad \text{and} \quad \underset{(\mathcal{K}, K, \phi)}{\operatorname{argmin}} \widetilde{\mathcal{F}}_\alpha(\mathcal{K}, K, \phi) = \underset{(\mathcal{K}, K, \phi)}{\operatorname{argmin}} \mathcal{L}_\alpha(\mathcal{K}, K, \phi; \bar{\lambda}, \mu). \quad (14)$$

Alternatively, such a vector $\bar{\lambda}$ is said to support an exact penalty representation for the problem of minimizing \mathcal{F}_α under the constraints $\mathcal{W}(\phi) = 0$ and $M(\mathcal{K}, K) = 0$, see for example [7].

In order to prove the main result of this subsection, we shall first present some preliminary results concerning Definition 1.

Lemma 1. *The following assertions hold true:*

- i) For any $(\lambda, \mu) \in (L^2(\Omega))^2 \times \mathbb{R}_+$ the function $\rho(\cdot, \lambda, \mu)$ is upper semi-continuous at 0 and satisfies $\rho(0, \lambda, \mu) = 0$.
- ii) For each $z \in (L^2(\Omega))^2$ and $\lambda \in (L^2(\Omega))^2$, the function $\rho(z, \lambda, \cdot)$ is monotonically decreasing in \mathbb{R}_+ .
- iii) For every neighborhood $V \subset (L^2(\Omega))^2$ of $z = 0$ and for every $(\lambda, \bar{\mu}) \in (L^2(\Omega))^2 \times \mathbb{R}_+$, it holds
 - a) $A_{\lambda, \bar{\mu}}^V(\mu) := \inf_{z \in V^c} \{\rho(z, \lambda, \bar{\mu}) - \rho(z, \lambda, \mu)\} > 0, \forall \mu > \bar{\mu};$
 - b) $\lim_{\mu \rightarrow \infty} A_{\lambda, \bar{\mu}}^V(\mu) = \infty.$

Proof. The continuity and monotonicity of ρ as well as the fact that $\rho(0, \lambda, \mu) = 0$ are direct consequences of the definition of the coupling function ρ (see Definition 1, item 6). This proves assertions i) and ii). Assertion iii) follows from the identity $\rho(z, \lambda, \bar{\mu}) - \rho(z, \lambda, \mu) = (\mu - \bar{\mu})\|z\|$. \square

In the sequel, we demonstrate certain characteristics of the perturbation function θ . We start by introducing the Fenchel-Moreau conjugate and biconjugate functions, as well as the abstract subgradient.

Definition 3 ([27, Chapter 11]). *The Fenchel–Moreau conjugated and biconjugated functions of θ with respect to the coupling function ρ are defined respectively by*

$$\theta^\rho(\lambda, \mu) = \sup_{z \in (L^2(\Omega))^2} \{\rho(z, \lambda, \mu) - \theta(z)\} \quad \text{and} \quad \theta^{\rho\rho}(z) = \sup_{(\lambda, \mu) \in (L^2(\Omega))^2 \times \mathbb{R}_+} \{\rho(z, \lambda, \mu) - \theta^\rho(\lambda, \mu)\}.$$

Moreover, given $\epsilon \geq 0$, an element $(\lambda, \mu) \in (L^2(\Omega))^2 \times \mathbb{R}_+$ is called ϵ -abstract subgradient of θ at \bar{z} with respect to ρ when $\theta(z) - \rho(z, \lambda, \mu) \geq \theta(\bar{z}) - \rho(\bar{z}, \lambda, \mu) - \epsilon$, for all $z \in (L^2(\Omega))^2$. The set of all ϵ -abstract subgradients of θ at \bar{z} is called ϵ -subdifferential of θ at \bar{z} and is denoted by $\partial_{\rho, \epsilon}\theta(\bar{z})$.

Lemma 2. *Consider the perturbation function θ as in Definition 1*

- i) *The perturbation function θ is lsc at $z = 0$.*
- ii) *Moreover, from the definitions of θ^ρ and $\theta^{\rho\rho}$ it follows that $\text{dom}(\theta^\rho) \neq \emptyset$, $\theta^\rho(\lambda, \mu) = -Q(\lambda, \mu)$ and $\theta^{\rho\rho}(z) \leq \theta(z)$.*
- iii) *The weak duality property is true, that is, $V_d \leq V_p$.*

Proof. Item i) and ii) are direct consequences of Definition 2 and Definition 3, respectively. To prove item iii), first observe that $\rho(0, \lambda, \mu) = 0$ from Lemma 1 i). Utilizing this fact in Definition 3, and item ii), we can deduce that $\theta^{\rho\rho}(0) = V_d \leq \theta(0) = V_p$. \square

We finally check the last supporting result before continuing to demonstrate the primary theorem of this subsection.

Lemma 3. *Let ρ and θ as in Definition 2. Furthermore, consider the ϵ -subgradient as in Definition 3. Then:*

- a) *If $(\lambda, \mu_0) \in \partial_{\rho, \epsilon}\theta(0)$, then $(\lambda, \mu) \in \partial_{\rho, \epsilon}\theta(0)$, for every $\mu \geq \mu_0$.*
- b) *For all $\epsilon > 0$ it holds $\partial_{\rho, \epsilon}\theta(0) \neq \emptyset$.*
- c) *Let $(\bar{\lambda}, \bar{\mu}) \in \text{dom}(\theta^\rho)$ be given. For every $\epsilon > 0$ there exists a $\mu_0 = \mu_0(\epsilon)$ such that $(\bar{\lambda}, \mu) \in \partial_{\rho, \epsilon}\theta(0)$, for all $\mu \geq \mu_0$.*

d) Let $(\bar{\lambda}, \bar{\mu}) \in \text{dom}(\theta^\rho)$ be given. There exists

$$\theta(z) \geq \theta(0) - \langle \bar{\lambda}, z \rangle - \hat{\mu} \|z\|_{L^2}, \quad \forall z \in (L^2(\Omega))^2.$$

Proof. The assertion of item a) is a consequence of the definition of the ϵ -abstract subgradient $\partial_{\rho, \epsilon} \theta(\cdot)$, in addition to Lemma 1 i) and ii).

Lemma 2-i) and ii) and Lemma 1 guarantee that the requirements of [23, Theorem 5.2.1] (see also [7]) are fulfilled, thus confirming the validity of items b) and c).

Finally, observe that item a) implies the existence of an element $(\bar{\lambda}, \bar{\mu})$ in the domain of θ^ρ . Define $\hat{\mu} := \max\{1, \|\bar{\lambda}\|\}$. Thus, the estimate $-\langle \bar{\lambda}, z \rangle - \hat{\mu} \|z\| \leq (\|\bar{\lambda}\| - \hat{\mu}) \|z\| \leq 0$ holds true for all $z \in (L^2(\Omega))^2$.

Given $\epsilon > 0$, we can deduce from the Definition 3 of ϵ -subgradient, the assertion in item c) of this lemma, the definition of ρ , and Lemma 1-i) that

$$\theta(z) - \rho(z, \bar{\lambda}, \mu_\epsilon) \geq \theta(0) - \rho(0, \bar{\lambda}, \mu_\epsilon) - \epsilon = \theta(0) - \epsilon \quad \forall z \in (L^2(\Omega))^2. \quad (15)$$

From Lemma 1-ii) and (15), it follows that $\theta(z) \geq \theta(0) - \langle \bar{\lambda}, z \rangle - \hat{\mu} \|z\|$ for all $z \in (L^2(\Omega))^2$, which concludes the proof. \square

Next, we prove the main result of this subsection: the zero-duality gap property for the proposed augmented Lagrangian approach. It should be noted that, as a result of Lemma 2-iii), this property is equivalent to $\theta^{\rho\rho}(0) = \theta(0)$.

Theorem 4. *Let the main assumptions **A1** - **A3** hold. Consider \mathcal{F}_α , \mathcal{W} and M be defined as above.*

(i) *There exists $\bar{\lambda} \in (L^2(\Omega))^2$ supporting an exact penalty representation in the sense of Definition 2.*

(ii) *There is no duality gap, i.e., $\theta^{\rho\rho}(0) = V_d = V_p = \theta(0)$.*

Proof. From Assumption **A3**), we conclude that the set of primal solutions is not empty. This implies that $\theta(0) < +\infty$ (see Definition 1, item 6). Additionally, Lemma 2-i) guarantees that the perturbation function θ is lower semi continuous at $z = 0$; consequently, $f(\mathcal{K}, K, \phi, \cdot)$ is also lower semi continuous at $z = 0$ for every $(\mathcal{K}, K, \phi) \in X$ (see Definition 1, item 5). Moreover, Lemma 1-i) and ii) implies that the coupling function $\rho(\cdot, \lambda, \mu)$ is upper semi continuous at $z = 0$, monotonically decreasing and satisfies $\rho(0, \lambda, \mu) = 0$ (see Definition 1, item-6).

On the other hand, Lemma 3 d) imply the existence of a $\hat{\mu} > 0$ satisfying

$$\theta(z) \geq \theta(0) - \langle \bar{\lambda}, z \rangle - \hat{\mu} \|z\|_{L^2}, \quad \forall z \in (L^2(\Omega))^2.$$

Thus, arguing with [7, Theorem 3] we conclude that Assertion (i) holds true.

A consequence of Assertion (i) is that

$$V_p = \theta^{\rho\rho}(0) = Q(\bar{\lambda}, \mu) \leq \sup_{(\lambda, \mu)} Q(\lambda, \mu) = \theta(0) = V_d.$$

This inequality combined with the weak duality property (13) allow us to conclude that Assertion (ii) holds. \square

3.2 Convergence analysis for the double well (PCLS) approach

In this subsection, we investigate regularization properties of the minimizers of the augmented Lagrangian approach proposed in this manuscript (see Theorem 5). The proofs of these results are analogous to the ones presented in [2, Theorems 4, 5, 6]; for the convenience of the reader, only a sketch is presented.

Theorem 5. Under the assumptions of Theorem 4, for any $\alpha > 0$, we have:

- i) The functional $\widetilde{\mathcal{F}}_\alpha$ attains minimizer on the set of admissible functions satisfying the constraints $\mathcal{W}(\phi) = 0$ and $M(\mathcal{K}, K) = 0$.
- ii) Problem (10) has a solution in the set of admissible functions.
- iii) Let $\bar{\lambda}_\alpha$ supporting an exact penalty representation and $\mu_\alpha > \bar{\mu}_\alpha$ as in Definition 2 (the existence follows from Theorem 4). Then, the augmented Lagrangian $\mathcal{L}_\alpha(\cdot; \bar{\lambda}_\alpha, \mu_\alpha)$ attains a minimizer on the set of admissible functions.
- iv) A solution of the problem (10) can be obtained by solving the unconstrained optimization problem $\min_{(\mathcal{K}, K, \phi)} \mathcal{L}_\alpha(\mathcal{K}, K, \phi; \bar{\lambda}_\alpha, \mu_\alpha)$.
- v) [Convergence] Assume that we have exact data, i.e. $\delta = 0$ in (4). For every $\alpha > 0$ let $(\mathcal{K}_\alpha, K_\alpha, \phi_\alpha)$ be a corresponding minimizer of $\mathcal{L}_\alpha(\cdot; \bar{\lambda}_\alpha, \mu_\alpha)$ in the set of admissible functions (the existence is guaranteed by item (iii) above). Then, for every sequence of positive numbers $\{\alpha_j\}$ converging to zero, the corresponding sequence $\{\mathcal{K}_{\alpha_j}, K_{\alpha_j}, \phi_{\alpha_j}\}$ of minima of $\mathcal{L}_{\alpha_j}(\cdot; \bar{\lambda}_{\alpha_j}, \mu_{\alpha_j})$ has a subsequence (which we denote by the same index) $\{\mathcal{K}_{\alpha_j}, K_{\alpha_j}, \phi_{\alpha_j}\}$ that is strongly convergent in $(L^2(\Omega))^2 \times L^p(\Omega)$, for $1 \leq p$. The limit of $\{\mathcal{K}_{\alpha_j}, K_{\alpha_j}, \phi_{\alpha_j}\}$ is an admissible function. Moreover, it is a solution of (7) with $y^\delta = y$.
- vi) [Stability] Let $\alpha = \alpha(\delta)$ be a positive function such that $\lim_{\delta \rightarrow 0} \alpha(\delta) = 0$ and $\lim_{\delta \rightarrow 0} \delta^2/\alpha(\delta) = 0$. Moreover, let $\{\delta_j\}$ be a sequence of positive numbers converging to zero and $\{y^{\delta_j}\} \in Y$ be the corresponding noisy data satisfying (4). Then, there exists a subsequence, denoted again by $\{\delta_j\}$, and a sequence $\{\alpha_j := \alpha(\delta_j)\}$ such that the corresponding minimizers $(\mathcal{K}_{\alpha_j}, K_{\alpha_j}, \phi_{\alpha_j})$ of $\mathcal{L}_{\alpha_j}(\cdot; \bar{\lambda}_{\alpha_j}, \mu_{\alpha_j})$ converges in $(L^2(\Omega))^2 \times L^p(\Omega)$, for $1 \leq p$ to a solution of (7) with $y^\delta = y$.

Sketch of the Proof: Assertion i) follows similarly to Lemma 3 in [2], where the continuity of $B(\cdot, \cdot)$ is given by Proposition 9, presented in the appendix. Assertion ii) follows immediately from Assertion i) and the definition of $\widetilde{\mathcal{F}}_\alpha$ (see Definition 1). Assertion iii) follows from Assertion i) and (14). Assertion iv) follows from Theorem 4 and Assertions ii) and iii). The proofs of Assertions v) and vi) follow the lines of [2, Theorems 5 and 6], respectively.

4 Numerical experiments

In this section, we investigate the performance and limitations of the augmented Lagrangian PCLS regularization method introduced in Section 2 for solving the semi-blind deconvolution problem arising in barcode decoding. To this end, we introduce an ADMM-type algorithm [5] to compute a primal-dual solution for the augmented Lagrangian

$$\begin{aligned}
\tilde{L}_\alpha(\tilde{\sigma}, \sigma, \phi; \lambda, \mu) := & \|B(K(\sigma), \phi) - y^\delta\|_{L^2(\Omega)}^2 \\
& + \alpha(\beta_1(\|\mathcal{K}(\tilde{\sigma}) - K_0\|_{H^1(\Omega)}^2 + \|K(\sigma) - K_0\|_{H^1(\Omega)}^2) + \beta_2 \|\phi\|_{L^{4n}}^2 + \beta_3 |\phi|_{\text{BV}}) \\
& + \langle \lambda_1, M(\mathcal{K}(\tilde{\sigma}), K(\sigma)) \rangle_{L^2(\Omega)} + \langle \lambda_2, \mathcal{W}(\phi) \rangle_{L^2(\Omega)} \\
& + \mu(\beta_4 \|M(\mathcal{K}(\tilde{\sigma}), K(\sigma))\|_{L^2(\Omega)} + \|\mathcal{W}(\phi)\|_{L^2(\Omega)}). \tag{16}
\end{aligned}$$

Here, $\mathcal{K}(\tilde{\sigma}) := \mathcal{K}(\tilde{\sigma})(x) = \gamma(\tilde{\sigma}\sqrt{2\pi})^{-1}e^{-(x^2/(2\tilde{\sigma}^2))}\chi_\Omega(x)$, $K(\sigma) := K(\sigma)(x) = \gamma(\sigma\sqrt{2\pi})^{-1}e^{-(x^2/(2\sigma^2))}\chi_\Omega(x)$, $K_0 = K_0(x)$ is the *a priori* in (9), and α, β_i are positive constants.

4.1 An algorithm for the augmented Lagrangian PCLS regularization method

In what follows, we detail the primal-dual iterative algorithm employed in our numerical experiments. Let $\sigma_0, \tilde{\sigma}_0 \in \mathbb{R}_+$, $\phi_0 \in L^2(\Omega)$, $\lambda_0 = ((\lambda_1)_0, (\lambda_2)_0) \in (L^2(\Omega))^2$ and $\mu_0 \in \mathbb{R}_+$ be given.

Algorithm 1

- 1 Update primal variables $(\tilde{\sigma}_k, \sigma_k, \phi_k)$
 - 1.1 $\phi_{k+1} \in \arg \min_{\phi} \tilde{L}_{\alpha}(\tilde{\sigma}_k, \sigma_k, \phi; \lambda_k, \mu_k)$
 - 1.2 $(\tilde{\sigma}_{k+1}, \sigma_{k+1}) \in \arg \min_{(\tilde{\sigma}, \sigma)} \tilde{L}_{\alpha}(\tilde{\sigma}, \sigma, \phi_{k+1}; \lambda_k, \mu_k)$
 - 2 Update dual variables (λ_k, μ_k)
 - 2.1 $(\lambda_1)_{k+1} = (\lambda_1)_k + a_{\lambda} M(K(\sigma_{k+1}), \mathcal{K}(\tilde{\sigma}_{k+1}))$
 - 2.2 $(\lambda_2)_{k+1} = (\lambda_2)_k + \frac{a_{\lambda}}{\|\mathcal{W}(\phi_{k+1})\|^2 + \varepsilon} \mathcal{W}(\phi_{k+1})$
 - 2.3 $\mu_{k+1} = \mu_k + \frac{a_{\mu}}{(\|\mathcal{W}(\phi_{k+1})\| + \beta_4 \|M(K(\sigma_{k+1}), \mathcal{K}(\tilde{\sigma}_{k+1}))\|)^2 + \varepsilon} (\|\mathcal{W}(\phi_{k+1})\| + \beta_4 \|M(K(\sigma_{k+1}), \mathcal{K}(\tilde{\sigma}_{k+1}))\|)$
-

where a_{λ} , a_{μ} , and ε are positive constants (ε small). Algorithm 1 is terminated when the constraints $\|\mathcal{W}(\phi_k)\| = 0$ and $\|M(\mathcal{K}(\tilde{\sigma}_k), K(\sigma_k))\| = 0$ are simultaneously satisfied within a prescribed accuracy.

Remark 4 (Update of the primal and dual variables in Algorithm 1).

- *Update of the primal variables $(\tilde{\sigma}, \sigma, \phi)$: To solve the optimization problems in Step 1 of Algorithm 1, we proceed as follows:¹*

In Step 1.1, the BFGS method [8] is employed to solve the minimization problem with respect to ϕ . We use the limited-memory variant, referred to as Limited-memory BFGS (L-BFGS-B),² which exploits the a priori information that the barcode values ϕ are constrained to lie in $[0, 1]$.

In Step 1.2, the CG method [17] is used to solve the minimization problem with respect to $(\tilde{\sigma}, \sigma)$.³

- *Update of the dual variables $(\lambda_1, \lambda_2, \mu)$:*

In Step 2.1, we use a gradient method with constant stepsize a_{λ} to update λ_1 .

In Steps 2.2 and 2.3, to avoid slow convergence (close to the solution) of the gradient method, we use a variant of the normalized gradient method [29] (see also [25, Chapter 3.3.4] to update λ_2 and μ respectively. A small positive constant ε is added in the denominator to enhance stability and to limit the step size when the gradient becomes small.

4.2 Numerical setup for the barcode recovering problem

The ground-truth barcode \hat{u} used in our numerical experiments is depicted in Figure 1 (TOP). This barcode is the same as that employed in the numerical simulations presented in [14]. Following the ansatz in (6), \hat{u} is modeled by a function $\hat{\phi} : [-1, 1] \rightarrow \mathbb{R}$, where $\hat{\phi}(x) = 0$ corresponds to the black bars and $\hat{\phi}(x) = 1$ corresponds to the white spaces between the bars, for all $x \in [-1, 1]$; see Figure 1 (BOTTOM).

As explained in the Introduction, the barcode recovery problem consists in simultaneously identifying the pair $(\hat{u}, \hat{\sigma})$ from noisy data. In each experiment, the barcode \hat{u} is corrupted by a convolution with the PSF kernel K defined in (2), using a known standard deviation $\hat{\sigma}$, followed by the addition of uniformly distributed noise satisfying (4). To illustrate the numerical setup of this inverse problem we show in Figure 1 the scenario corresponding to $\hat{\sigma} = 0.026$ and $\delta = 0.5\%$.

¹Both Steps 1.1 and 1.2 are implemented using the Python library SciPy [32] with its default parameters.

²See <https://docs.scipy.org/doc/scipy/reference/generated/scipy.optimize.minimize.html>

³See <https://docs.scipy.org/doc/scipy/reference/generated/scipy.sparse.linalg.cg.html>

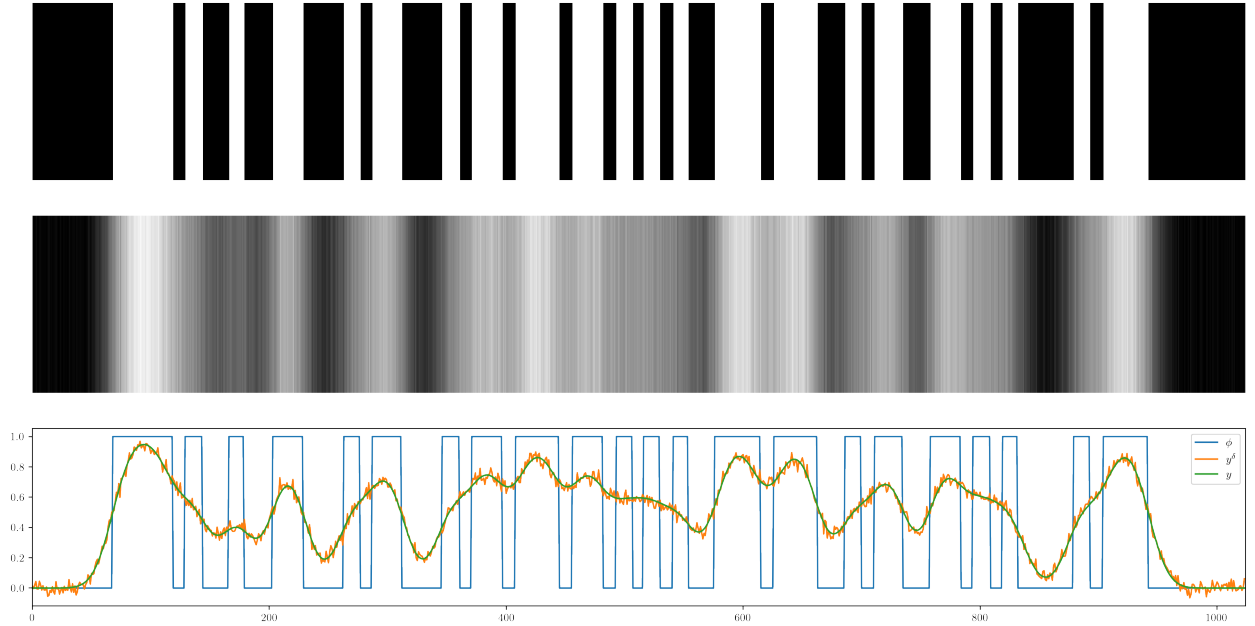


Figure 1: Numerical setup for the barcode recovery problem ($\hat{\sigma} = 0.026$ and $\delta = 0.5\%$): (TOP) ground-truth barcode \hat{u} ; (CENTER) observed signal obtained from exact barcode by convolution with a Gaussian kernel followed by the addition of noise; (BOTTOM) functions $\hat{\phi}$ (modeling the barcode \hat{u}), y (exact data obtained by convolving $\hat{\phi}$ with the PSF kernel) and y^δ (noisy data).

Three distinct variances levels ($\hat{\sigma}^2$) are considered in our experiments, namely $\hat{\sigma} = 0.024$, $\hat{\sigma} = 0.026$, and $\hat{\sigma} = 0.028$. For each of these values, two levels of relative noise are examined, namely $\delta = 0.5\%$ and $\delta = 5.0\%$ (an additional experiment with $\delta = 10\%$ is also considered; see Figures 8 and 9).

Remark 5 (On the physical interpretation of the experiments). *There is no universal relation of the form $d = f(\sigma)$ that directly links the scanner-barcode distance d to the standard deviation σ without introducing an additional physical model or a calibration procedure.*

The model adopted in (2) relies on the qualitative assumption $\sigma = \kappa dL$, where L denotes the barcode width and κ is a system-dependent constant (physically, the constant κ is directly related to the angular divergence of the laser beam). Datasheets of commercial laser modules and low-cost 1D barcode scanners (e.g., Zebra Technologies / Symbol and Datalogic devices commonly used in supermarkets) indicate that the total angular divergence of the laser beam typically ranges between 0.004 and 0.015 radians. Consequently, calibrated values of κ are generally expected to lie on the order of 10^{-3} .

In our setting, the computational domain is normalized to $\Omega = (-1, 1)$. We assume a typical barcode width of $L = 3\text{cm}$ (e.g., an EAN-13 code, which is widely used in retail environments), and further assume that representative values of κ for commercial (low-cost) barcode scanners (e.g., supermarket scanners) lie within the range: $\kappa \in (0.002, 0.003)$. Therefore, for low-cost scanners, the range $\sigma \in (0.024, 0.028)$ considered in our experiments corresponds to a physical scanner-barcode distance of approximately $d \in (24\text{cm}, 42\text{cm})$.

4.3 Implementation aspects of Algorithm 1

The function $\hat{\phi}$, modeling the ground-truth barcode \hat{u} , is discretized on a uniform mesh of 1024 equally spaced points on the interval $[-1, 1]$. This same mesh is used to represent the regularized solutions in all experiments conducted in this section.

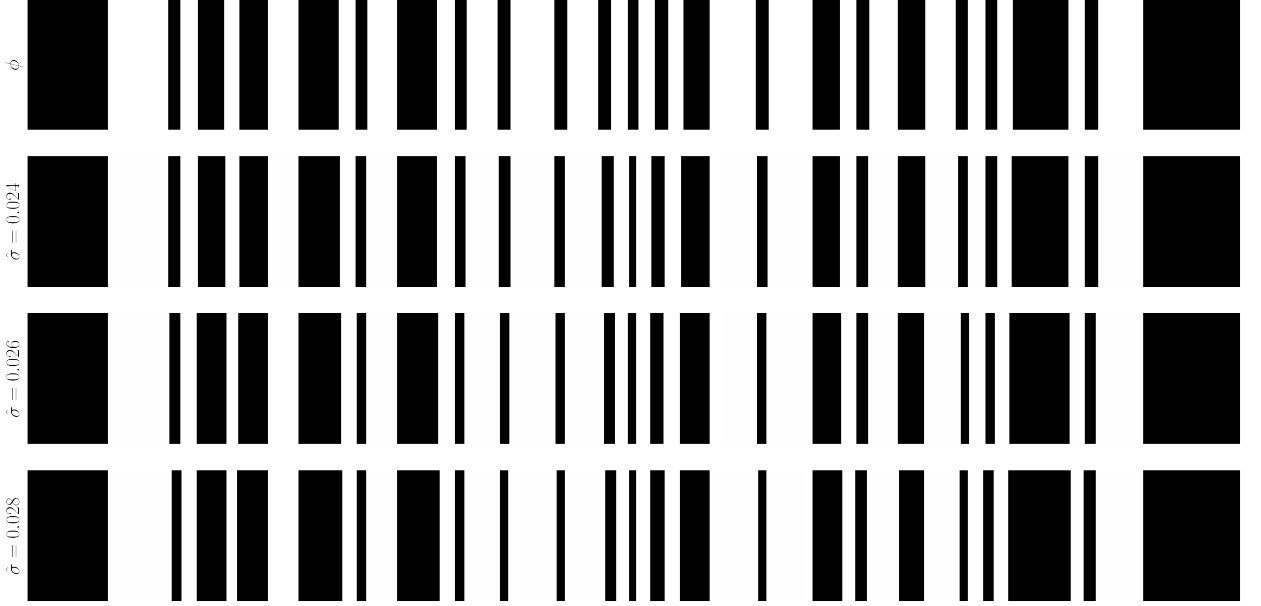


Figure 2: Reconstructed barcodes for $\delta = 0.5\%$ and different values of $\hat{\sigma}$.

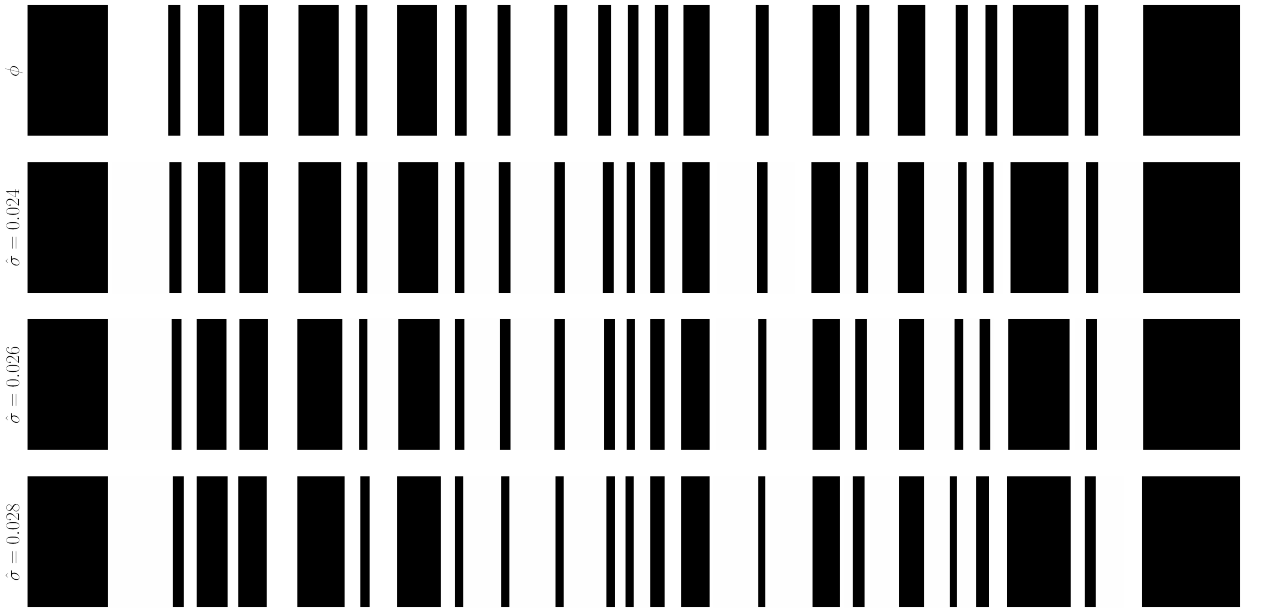


Figure 3: Reconstructed barcodes for $\delta = 5\%$ and different values of $\hat{\sigma}$.

The double-well $\mathcal{W}(\phi) := \phi^n(\phi - 1)^n$ in (7) is chosen with $n = 2$. In the simulations, the regularization parameter is set to $\alpha = 10^{-8}$, while the scaling factors β_j in (16) are chosen as $\beta_1 = \beta_3 = 10^{-8}$, $\beta_2 = 1$, $\beta_4 = 0.02$, and the constant ε is set to 10^{-10} .

As initial guess ϕ_0 for Algorithm 1 we set $\phi_0(x) \equiv 0.1$, i.e., a constant function representing an almost completely black barcode. We assume that the amplitude of the kernel K is $\gamma = 1$. The initial guess $\sigma_0 \in \mathbb{R}_+$ for the standard deviation of the kernel $K_0 = \overline{K}(\sigma_0)$ is set to $\sigma_0 = 0.02$. The initial guess for the standard deviation associated with the slack variable \mathcal{K} is set to $\tilde{\sigma}_0 = 10^{-3}$, which corresponds to a low-intensity blurring.

As initial guess for the dual variables (λ, μ) of the augmented Lagrangian we use the values $\mu_0 = 0.04$ and $\lambda_0(x) = (0, 0)$. The constants $a_\mu = a_\lambda = 0.0004$ are used in the implementation of Step 2.

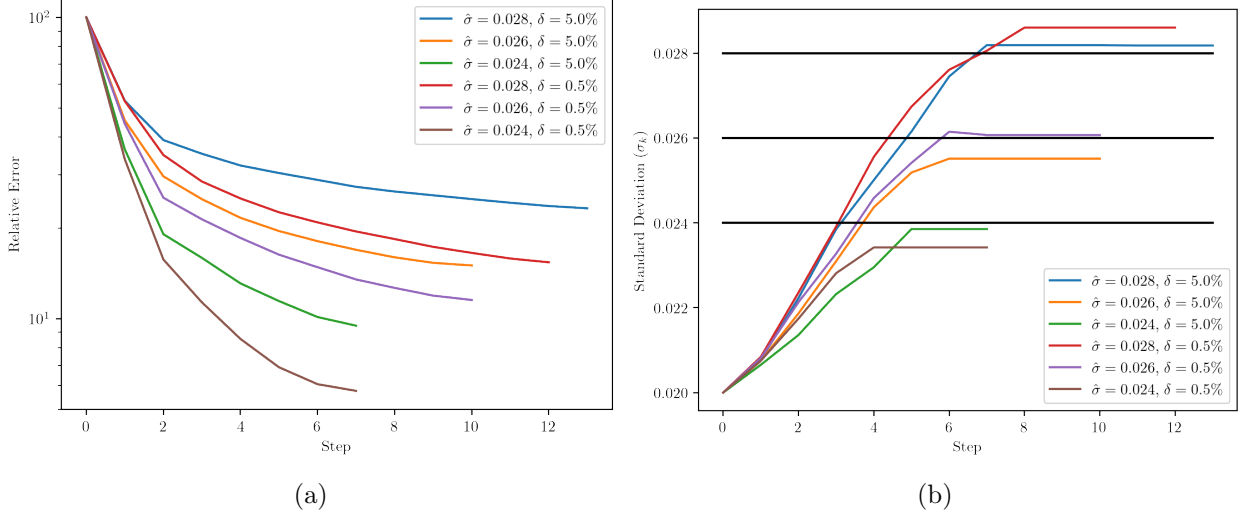


Figure 4: (a) Relative error (L^1 -norm) and (b) evolution of reconstructed σ_k for all experiments.

As stopping criteria, Algorithm 1 is terminated when both conditions

$$\|\mathcal{W}(\phi_k)\|_{L^1(\Omega)} \leq 10^{-5} \quad \text{and} \quad \|\mathcal{M}(K(\sigma_k), \mathcal{K}(\tilde{\sigma}_k))\|_{L^1(\Omega)} \leq 10^{-5}$$

are simultaneously satisfied.

4.4 Numerical reconstructions

In what follows, we discuss the performance of Algorithm 1 in Section 4.1 for the semi-blind deconvolution problem of simultaneously identifying the barcode \hat{u} and the variance $\hat{\sigma}^2$. We test the method in three distinct scenarios corresponding to blurred barcodes with standard deviations $\hat{\sigma} = 0.024$, $\hat{\sigma} = 0.026$ and $\hat{\sigma} = 0.028$. In each scenario, we consider noisy measurements y^δ , contaminated with noise levels $\delta = 0.5\%$ and $\delta = 5\%$.

The reconstruction results shown in Figure 2 (for $\delta = 0.5\%$) and Figure 3 (for $\delta = 5\%$) demonstrate the potential of Algorithm 1 to recover both the widths and the positions of the bars and gaps in the ground-truth barcode \hat{u} , across all considered scenarios of blur $\hat{\sigma}$, which ranges over the interval $\hat{\sigma} \in [0.024, 0.028]$. To complement the discussion of the results shown in these two figures, Figure 4 presents two plots that are relevant for assessing the efficiency of Algorithm 1: (i) Figure 4a shows the evolution of the **relative iteration error**

$$\|\phi_k - \hat{\phi}\|_{L^1} / \|\hat{\phi}\|_{L^1},$$

for the six experiments presented in Figures 2 and 3 (corresponding to three different values of the variance $\hat{\sigma}^2$ and two distinct noise levels δ); (ii) Figure 4b displays the evolution of the iterated values σ_k corresponding to the same experiments examined in Figure 4a.

It is important to note that Algorithm 1 is capable of producing reasonable approximations of the ground-truth barcode after only a few iterations. To illustrate this finding, we detail the barcode sequences generated by Algorithm 1 in two distinct scenarios: (i) Figure 5, corresponding to $\hat{\sigma} = 0.024$ and $\delta = 0.5\%$; (ii) Figure 6, corresponding to $\hat{\sigma} = 0.028$ and $\delta = 5\%$. In both experiments, the algorithm yields a sufficiently accurate approximation of the ground-truth barcode after only three iterations.

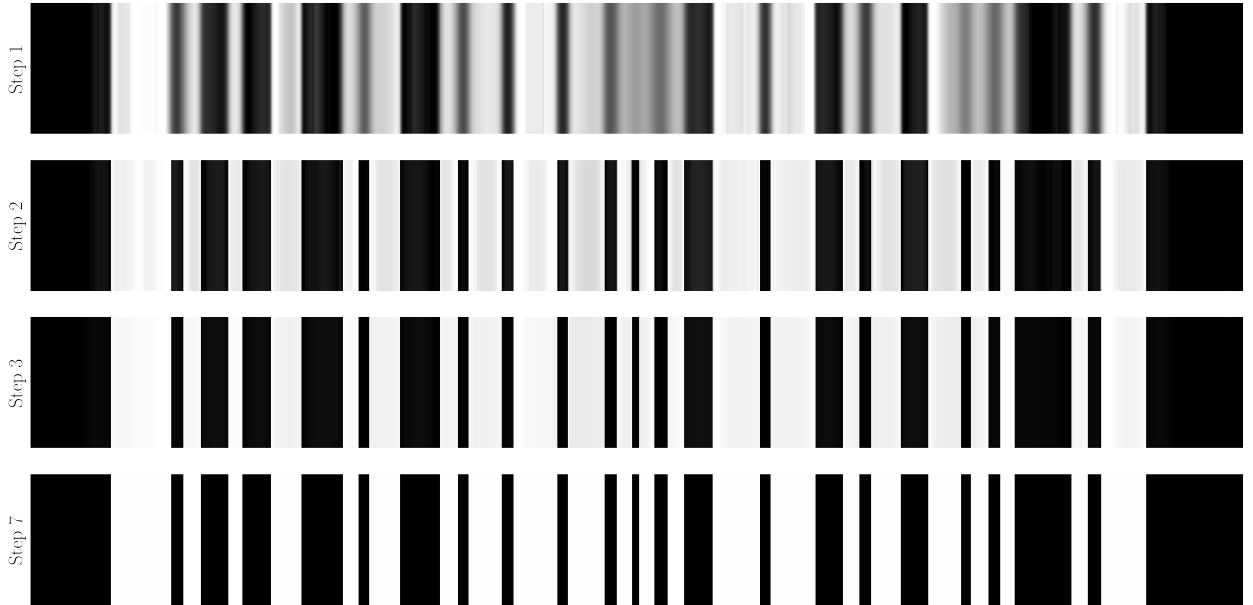


Figure 5: Evolution of reconstructed barcode for $\hat{\sigma} = 0.024$ and $\delta = 0.5\%$

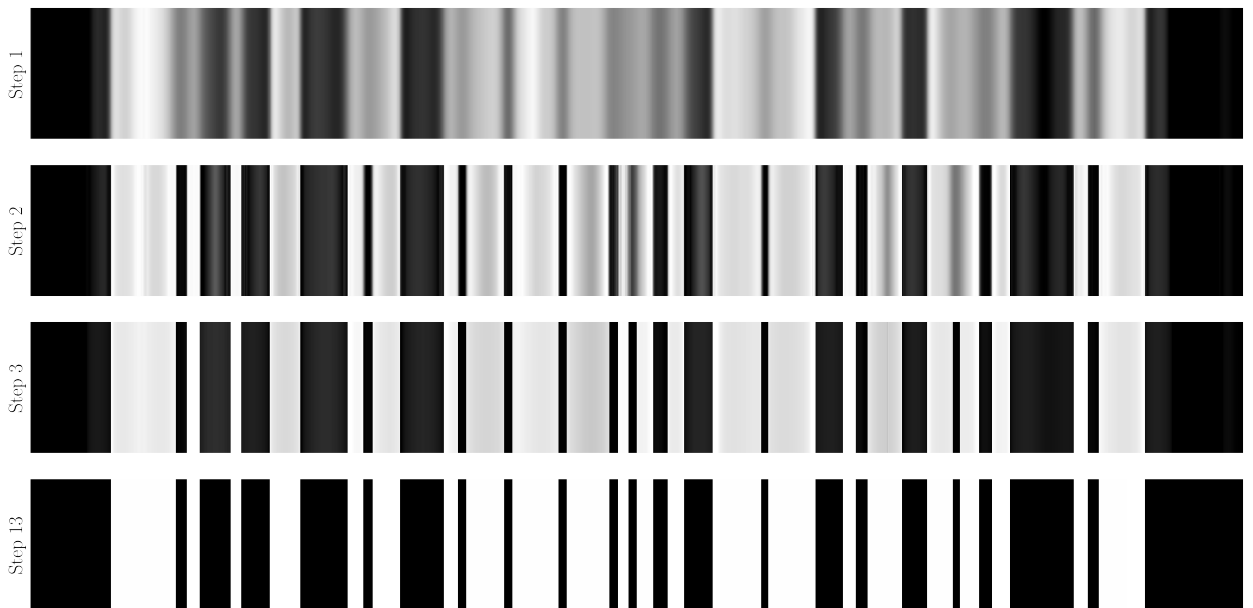


Figure 6: Evolution of reconstructed barcode for $\hat{\sigma} = 0.028$ and $\delta = 5\%$

In Figure 7, we present in detail the reconstruction results obtained for the scenario $\hat{\sigma} = 0.028$ (large variance) and $\delta = 5\%$ (high noise level).⁴ This represents the most unfavorable scenario for which Algorithm 1 was still able to produce reasonably reliable reconstructions, without loss of bars, significant positional shifts, or the generation of spurious bars.

We conclude this section by presenting a discussion of the main findings obtained from the numerical experiments reported in this manuscript.

- **Influence of variance values in the reconstruction:** Different values of the blur σ have a strong impact on the reconstruction quality. As the standard deviation increases from $\hat{\sigma} = 0.024$ to $\hat{\sigma} = 0.028$ the quality of the reconstructed barcode progressively degrades, meaning that the

⁴The bottom plot in Figure 6 corresponds to the third plot from the top in Figure 7.

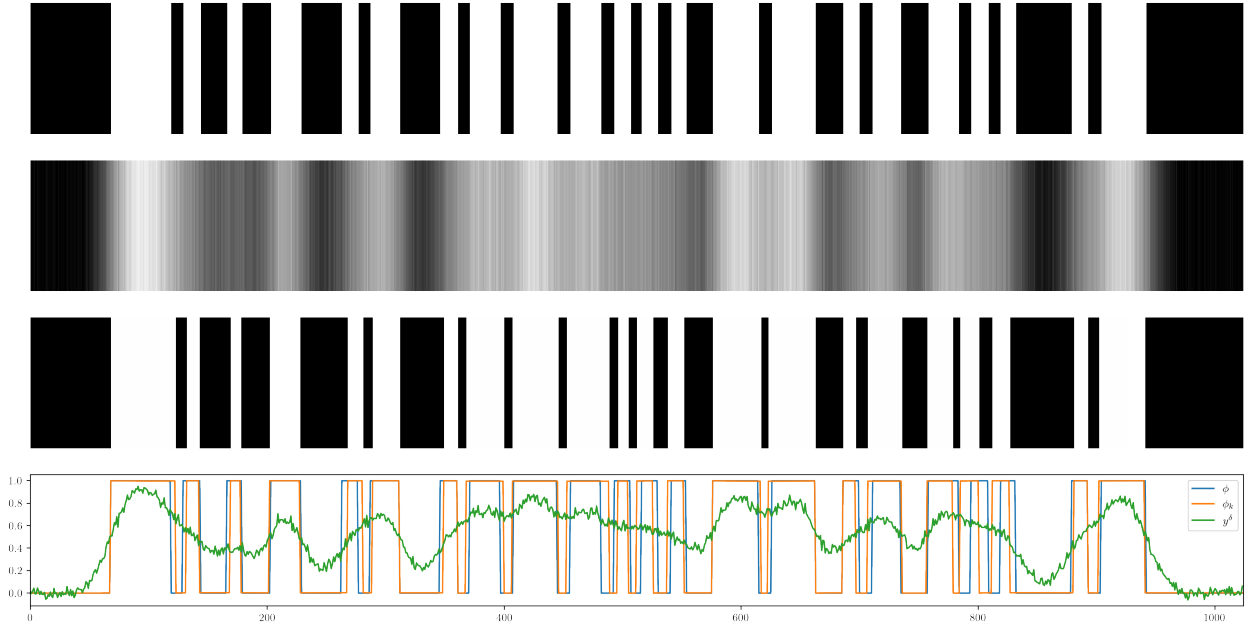


Figure 7: Scenario $\hat{\sigma} = 0.028$ and $\delta = 5\%$. From top to bottom: (1) ground-truth barcode \hat{u} ; (2) noisy data y^δ ; (3) reconstructed barcode; (4) functions $\hat{\phi}$, ϕ_k for $k = 7$, and y^δ

width and position of the reconstructed barcode bars become increasingly inaccurate.

For larger values of $\hat{\sigma}$, the thin black bars in \hat{u} tend to become progressively thinner and spatially displaced in the reconstructed barcode; as expected, this effect becomes more pronounced for higher levels of noise in the data (see Figures 2 and 3 and compare the distinct reconstructions corresponding to the same values of $\hat{\sigma}$).

From Figure 4a, it is clear that the relative iteration error $\|\phi_k - \hat{\phi}\|_{L^1} / \|\hat{\phi}\|_{L^1}$ attains smaller values at the end of the iteration (when the stopping criterion is met) for smaller values of $\hat{\sigma}$, indicating a higher accuracy of the reconstructed barcode. In Figure 4a, compare the BLUE and RED curves (corresponding to the standard deviation $\hat{\sigma} = 0.028$ for noise levels $\delta = 5.0\%$ and $\delta = 0.5\%$, respectively) with the GREEN and BROWN curves (corresponding to the standard deviation $\hat{\sigma} = 0.024$ for noise levels $\delta = 5.0\%$ and $\delta = 0.5\%$, respectively).

For values larger than $\sigma = 0.028$, Algorithm 1 fails to produce reliable reconstructions (independent of the noise level). In this regime, the reconstructed barcode tends to lose bars (particularly the thinner ones) or to produce spurious bars that are not present in the ground-truth barcode.

- **Influence of the noise level in the reconstruction:** Increasing the noise intensity δ has a less pronounced effect on the quality of the reconstructed barcode than increasing the parameter σ . This behavior is clearly illustrated in Figure 4a.

Our experiments indicate that when noise level exceeds 10% and the standard deviation exceeds $\sigma = 0.026$, Algorithm 1 fails, leading to the disappearance of bars and the emergence of spurious thin bars. For a concrete example we present in Figure 8 the details of the barcode reconstruction in the scenario $\hat{\sigma} = 0.028$ and $\delta = 10\%$. Additionally, in Figure 9, we show the reconstructed barcodes for $\delta = 10\%$ and different values of exact variance $\hat{\sigma}^2$.

- **Choice of the initial guess σ_0 :** Experimental results indicate that choosing a small value for the initial guess σ_0 leads to improved performance of the iterative algorithm. When σ_0 is large, the iterates ϕ_k tend to lose thin bars or to develop new spurious thin bars as the algorithm progresses. This behavior has also been reported in [14].

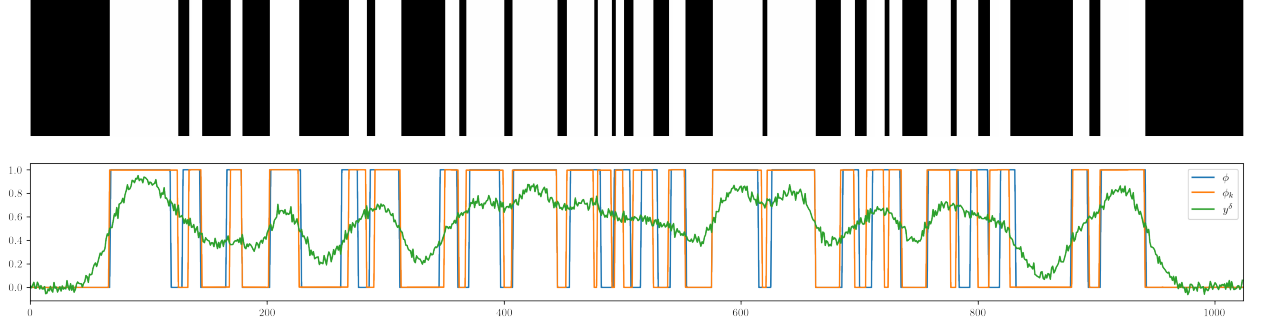


Figure 8: Scenario $\hat{\sigma} = 0.028$ and $\delta = 10\%$. (TOP) Reconstructed barcode; (BOTTOM) functions $\hat{\phi}$, ϕ_k for $k = 7$ and noisy data y^δ .

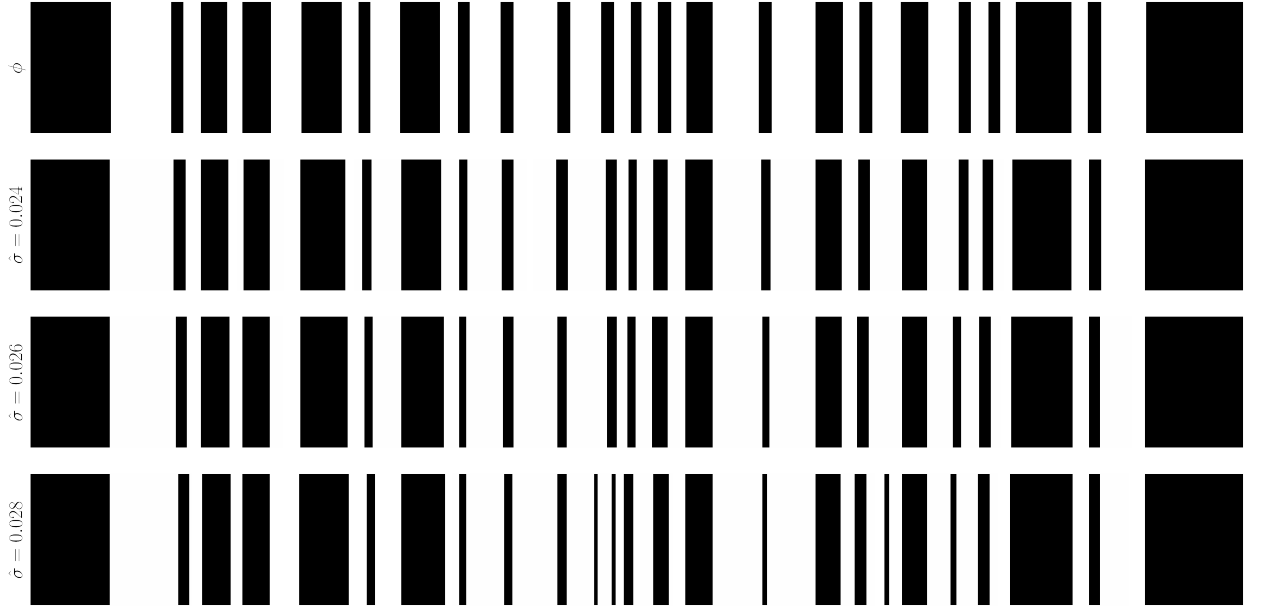


Figure 9: Barcode reconstructions for $\delta = 10\%$ and different values of variance values.

- **Fast convergence property:** Algorithm 1 is capable of successfully the locations and widths of the ground-truth bars and gaps at early stages of the iteration, typically between the second and third steps. Subsequent steps are mainly devoted to enforcing that the reconstructed values remain within the set $\{0, 1\}$.

For completeness, we illustrate this rapid convergence by examining the sequences generated by the method in two representative scenarios: (i) Figure 5, corresponding to $\hat{\sigma} = 0.024$ and $\delta = 0.5\%$; (ii) Figure 6, corresponding to $\hat{\sigma} = 0.028$ and $\delta = 5\%$.

In the vast majority of practical applications under consideration, the primary interest lies in the accurate identification of a binary barcode (the precise value of the variance is typically irrelevant to the end user). A fast and efficient strategy for accomplishing this task can be devised through the following two-step procedure:

- (I) Perform only $k = 3$ iterations of Algorithm 1, obtaining the approximation ϕ_3 (generally non-binary);
- (II) Apply a thresholding step to ϕ_3 in order to obtain a binary function $\tilde{\phi}_3$ (e.g., $\tilde{\phi}_3 = 1$ if $\phi_3 > 0.5$ and $\tilde{\phi}_3 = 0$ otherwise).

The function $\tilde{\phi}_3$ is then returned as an approximation of the unknown barcode. This strategy

exploits a characteristic behavior of Algorithm 1, namely its ability to produce reasonable (though not yet binary) approximations within only a few iterations. It thereby avoids the computational cost associated with a large number of additional iterations, whose primary purpose is to enforce binarity in the final reconstruction.

- **Recovery of variance values:** As shown in Figure 4b, the reconstruction of the true variance value becomes less accurate for large values of $\hat{\sigma}$, close to 0.028 (see the BLUE and RED curves). For small values of $\hat{\sigma}$, close to 0.024, the variance reconstruction is also inaccurate (see the GREEN and BROWN curves). The most accurate variance recovery is achieved for intermediate values of $\hat{\sigma}$, around 0.026 (see the ORANGE and PURPLE curves).

It is worth noting that accurate reconstructions of the ground-truth barcode can be obtained even in cases where the true standard deviation value $\hat{\sigma}$ is not accurately recovered. This behavior is illustrated by the reconstructions shown in Figures 2 and 3 for the cases $\hat{\sigma} = 0.024$ and $\hat{\sigma} = 0.028$.

- **Limitations of the proposed method:** Despite its effectiveness under moderate noise and variance levels, Algorithm 1 exhibits certain limitations. In particular, its performance deteriorates significantly when the variance parameter σ^2 exceeds specific thresholds, even in low-noise scenarios. Under such conditions, the algorithm fails to produce satisfactory reconstructions, leading to artifacts such as missing bars or the appearance of spurious thin bars (see for example Figures 8 and 9). Based on our experiments, we find that the reliability limit of the PCLS approach for the semi-blind deconvolution of the barcode \hat{u} is approximately $\sigma = 0.028$ for the standard deviation and $\delta = 5\%$ for the noise level. These findings are consistent with the results reported in [14].

5 Conclusions and future research

We adopt the (PCLS) framework, considered by the authors in [12], as a tool for addressing the semi-blind deconvolution problem arising in the decoding of blurred linear barcodes. By parameterizing the barcode u via a PCLS function ϕ and introducing a slack variable associated with the partially unknown convolution kernel K , we develop a solution strategy based on augmented Lagrangian techniques.

We establish several key theoretical results, most notably the existence of generalized multipliers for the augmented Lagrangian functional under consideration as well as the absence of duality gaps. These findings enable us to show that the primal solutions generated by the proposed augmented Lagrangian scheme provide stable approximate reconstructions of the underlying barcode in the associated inverse problem, even in the presence of noisy data.

We further conduct numerical experiments using an ADMM-type iterative algorithm, considering a range of variance parameters (governing the degree of blurring) and noise levels. The obtained results confirm the practical effectiveness of the proposed method, while also illustrating its limitations.

Potential directions for future research include extending the PCLS framework to the identification of 2D barcodes (e.g., QR code and Data Matrix), as well as to semi-blind deconvolution problems involving non-Gaussian kernels K .

Acknowledgements

ADC acknowledges support from FAPERGS (grant 123/2551-0001824-1) and CNPq (grant 401181/2025-1).

EH acknowledges support from DFG under Germany’s Excellence Strategy - EXC 2121 ”Quantum Universe” (grant 390833306) and CNPq (grant 163469/2021-0).

AL acknowledges support from CNPq (grant 307021/2025-4), FAPESC (grant 2024TR002238) and the AvH Foundation.

Appendix A: Auxiliary results

In this appendix, we recall some properties \mathcal{W} in appropriated topologies that are used in the manuscript. Analogous results can be found in [2, 12]. We present them here for sake of completeness. We also prove the point-wise continuity of the forward operator B .

First we briefly recall some basic facts about the space $\text{BV}(\Omega)$. For a proof we refer the reader to [16, Chapter 5].

Lemma 6. *The following assertions hold true:*

- i) *The semi-norm $|\cdot|_{\text{BV}}$ is weakly lower semi-continuous with respect to L^p -convergence, i.e. if $\{x_k\} \in \text{BV}(\Omega)$ converges to x in the L^p -norm, then $x \in \text{BV}(\Omega)$ and $|x|_{\text{BV}} \leq \liminf_{k \rightarrow \infty} |x_k|_{\text{BV}}$.*
- ii) *$\text{BV}(\Omega)$ is compactly embedded in $L^p(\Omega)$ for $1 \leq p < d/(d-1)$. Consequently, any bounded sequence $\{x_k\} \in \text{BV}(\Omega)$ has a subsequence converging in $L^p(\Omega)$ to some $x \in \text{BV}(\Omega)$. [EH: d?](#)*

The next lemma is devoted to the investigation of the relevant properties of operators \mathcal{W} . Such properties will be used throughout this paper.

Lemma 7. *Let the double-well operators \mathcal{W} defined in Section 1 and P_{pc} the operator defined in (6). For $1 \leq p < 2$, the following assertions hold true:*

i) \mathcal{W} is continuous maps from $L^{4n}(\Omega)$ to $L^2(\Omega)$

ii) If $\|\mathcal{W}(\phi)\|_{L^1} = 0$ or $\|\mathcal{W}(\phi)\|_{L^2} = 0$ for some $\phi \in L^{4n}(\Omega)$, then $\phi(x) \in \{0, 1\}$ a.e. in Ω .

Proof. The continuity of \mathcal{W} follows from the fact that

$$\begin{aligned} \int_{\Omega} (\mathcal{W}(\phi) - \mathcal{W}(\psi))^2 dx &= \int_{\Omega} (\phi^n - \psi^n)^2 (\phi - 1)^{2n} + 2(\phi^n - \psi^n)((\phi - 1)^n - (\psi - 1)^n)(\phi - 1)^n \psi^n dx \\ &\quad + \int_{\Omega} \psi^{2n}((\phi - 1)^n - (\psi - 1)^n)^2 dx, \end{aligned}$$

together with the fact that $(a^m - b^m) = (a - b)(a^{m-1} + a^{m-2}b + \dots + ab^{m-2} + b^{m-1})$, the Cauchy-Schwarz inequality and continuous embedding of $L^{4n}(\Omega)$ in $L^2(\Omega)$.

Assertions ii) follows immediately from the definition of \mathcal{W} . □

In the following lemma, we prove the weak continuity of the operator P_{pc} and the weak continuity on zero of \mathcal{W} .

Lemma 8. *Let the operator P_{pc} defined as in (6). Then:*

- i) *For any sequence $\{\phi_k\}$ of $L^{4n}(\Omega)$ with $\phi_k \rightharpoonup \phi$ in $L^{4n}(\Omega)$ (or $\phi_k \rightarrow \phi$ in $L^{4n}(\Omega)$), we have that $P_{pc}(\phi_k) \rightharpoonup P_{pc}(\phi)$ in (or $P_{pc}(\phi_k) \rightarrow P_{pc}(\phi)$) $L^2(\Omega)$. In particular, this result follows for the bar code decoding application, where P_{pc} is the identity.*
- ii) *For any sequence $\{\phi_k\}$ of $L^{4n}(\Omega)$ with $\phi_k \rightharpoonup \phi$ in $L^{4n}(\Omega)$ such that $\mathcal{W}(\phi_k) = 0$, we have that $\mathcal{W}(\phi) = 0$.*

Proof. Since Ω is bounded, we have that $L^{4n}(\Omega) \subset L^2(\Omega) \subset L^1(\Omega)$. Therefore, $\phi_k \rightharpoonup \phi$ (or $\phi_k \rightarrow \phi$) in $L^2(\Omega)$. Furthermore, $\phi_k \rightharpoonup \phi$ (or $\phi_k \rightarrow \phi$) in $L^1(\Omega)$.

By definition, the map P_{pc} is affine in $L^2(\Omega)$. Therefore, $P_{pc}(\phi_k) \rightharpoonup P_{pc}(\phi)$ (or $P_{pc}(\phi_k) \leftarrow P_{pc}(\phi)$) in $L^2(\Omega)$.

To prove Item ii), we remark that if $\mathcal{W}(\tilde{\phi}) = 0$ then $\tilde{\phi}(\tilde{\phi} - 1) = 0$ a.e.. The reciprocity is also true for any $\tilde{\phi} \in L^{4n}(\Omega)$. Now, the assertion follows from the weak convergence of ϕ_k in $L^2(\Omega)$ and Lemma 7 ii). \square

Next, we demonstrate the continuity of the forward operator B .

Proposition 9. *[Continuity of $B(\cdot, \cdot)$] Let the operator B be defined as in (5). Furthermore, let $(\mathcal{K}_k, K_k, \phi_k)$ and (\mathcal{K}, K, ϕ) be any vectors of admissible functions, i.e., satisfying Assumptions **A1**)-**A2**). If $K_k \rightarrow K$ in $L^2(\Omega)$ and $\phi_k \rightarrow \phi$ in $L^{4n}(\Omega)$, then $B(K_k, P_{pc}(\phi_k)) \rightarrow B(K, P_{pc}(\phi))$ in $L^2(\Omega)$.*

Proof. It follows from the assumptions and Lemma 8-i) that $P_{pc}(\phi_k)$ tends to $P_{pc}(\phi)$ in $L^2(\Omega)$. Since Ω is bounded, this convergence is also valid for $L^1(\Omega)$. Consequently, it follows from Young's inequality for convolution [1], Assumption **A1**), and the convergence of K_k to K in $L^2(\Omega)$ that

$$\begin{aligned} \|B(K_k, P_{pc}(\phi_k)) - B(K, P_{pc}(\phi))\|_{L^2(\Omega)} &= \|K_k * P_{pc}(\phi_k) - K * P_{pc}(\phi)\|_{L^2(\Omega)} \\ &\leq \|K_k * (P_{pc}(\phi_k) - P_{pc}(\phi))\|_{L^2(\Omega)} + \|(K_k - K) * P_{pc}(\phi)\|_{L^2(\Omega)} \\ &\leq \|K_k\|_{L^2(\Omega)} \|P_{pc}(\phi_k) - P_{pc}(\phi)\|_{L^1(\Omega)} + \|K_k - K\|_{L^2(\Omega)} \|P_{pc}(\phi)\|_{L^1(\Omega)}, \end{aligned}$$

concluding the assertion. \square

References

- [1] R. A. Adams, *Sobolev spaces*, Academic Press, New York, 1975.
- [2] J. P. Agnelli, A. De Cezaro, and A. Leitão, *A regularization method based on level sets and augmented lagrangian for parameter identification problems with piecewise constant solutions*, *Inverse Problems* **34** (2018), no. 12, 125003.
- [3] M. Bertero, P. Boccacci, and V. Ruggiero, *Inverse imaging with poisson data*, 2053-2563, IOP Publishing, 2018.
- [4] D.P. Bertsekas, *Constrained optimization and Lagrange multiplier methods*, Computer Science and Applied Mathematics, Academic Press, New York, 1982.
- [5] S. Boyd, N. Parikh, E. Chu, B. Peleato, and J. Eckstein, *Distributed optimization and statistical learning via the alternating direction method of multipliers*, *Foundations and Trends in Machine Learning* **3** (2011), no. 1, 1–122.
- [6] A. Buccini, M. Donatelli, and R. Ramlau, *A semiblind regularization algorithm for inverse problems with application to image deblurring*, *SIAM J. Sci. Comput.* **40** (2018), no. 1, A452–A483.
- [7] R.S Burachik, A.N. Iusem, and J.G. Melo, *Duality and exact penalization for general augmented lagrangians*, *J. Optim. Theory Appl.* **147** (2010), 125–140.
- [8] R. H. Byrd, P. Lu, J. Nocedal, and C. Zhu, *A limited memory algorithm for bound constrained optimization*, *SIAM Journal on Scientific Computing* **16** (1995), no. 5, 1190–1208.
- [9] R. Choksi and Y. van Gennip, *Deblurring of one dimensional bar codes via total variation energy minimization*, *SIAM Journal on Imaging Sciences* **3** (2010), no. 4, 735–764.

- [10] R. Choksi, Y. van Gennip, and A. Oberman, *Anisotropic total variation regularized l^1 -approximation and denoising/deblurring of 2d bar codes*, *Inverse Problems and Imaging* (2011), no. 5, 591–617.
- [11] A. De Cezaro and A. Leitão, *Level-set approaches of L_2 -type for recovering shape and contrast in ill-posed problems*, *Inverse Problems in Science and Engineering* **20** (2012), no. 4, 571–587.
- [12] A. De Cezaro, A. Leitão, and X.-C. Tai, *On piecewise constant level-set (pcls) methods for the identification of discontinuous parameters in ill-posed problems*, *Inverse Problems* **29** (2013), 015003.
- [13] H. W. Engl, M. Hanke, and A. Neubauer, *Regularization of inverse problems*, *Mathematics and its Applications*, vol. 375, Kluwer Academic Publishers Group, Dordrecht, 1996.
- [14] S. Esedoglu, *Blind deconvolution of bar code signals*, *Inverse Problems* (2004), no. 20, 121–135.
- [15] S. Esedoglu and F. Santosa, *Error estimates for a bar code reconstruction method*, *Discrete and Continuous Dynamical Systems Series B* **17** (2012), no. 6, 1889–1902.
- [16] L.C. Evans and R.F. Gariepy, *Measure theory and fine properties of functions*, *Studies in Advanced Mathematics*, CRC Press, Boca Raton, FL, 1992.
- [17] M. R. Hestenes and E. Stiefel, *Methods of conjugate gradients for solving linear systems*, *Journal of Research of the National Bureau of Standards* **49** (1952), no. 6, 409–436.
- [18] M. A. Iwen, F. Santosa, and R. Ward, *A symbol-based algorithm for decoding bar codes*, *SIAM Journal on Imaging Sciences* **6** (2013), no. 1, 56–77.
- [19] E. Joseph and T. Pavlidis, *Bar code waveform recognition using peak locations*, *IEEE Transactions on Pattern Analysis and Machine Intelligence* **16** (1994), no. 6, 630–640.
- [20] S. Krešić-Jurić, *Edge detection in bar code signals corrupted by integrated time-varying speckle*, *Pattern Recognition* **38** (2005), no. 12, 2483–2493.
- [21] Y. Lou, E. Esser, H. Zhao, and J. Xin, *Partially blind deblurring of barcode from out-of-focus blur*, *SIAM Journal on Imaging Sciences* **7** (2014), no. 2, 740–760.
- [22] X-G. Lv, J. Liu, F. Li, and X-L. Yao, *Blind motion deconvolution for binary images*, *Journal of Computational and Applied Mathematics* **393** (2021), 113500.
- [23] J.D.M. Melo, *On general augmented lagrangian and a modified subgradient algorithm.*, IMPA PhD Thesis, IMPA, Rio de Janeiro, RJ, 2009, pp. ix + 127.
- [24] L.K. Nielsen, X.-C. Tai, S.I. Aanonsen, and M. Espedal, *A binary level set model for elliptic inverse problems with discontinuous coefficients*, *Int. J. Numer. Anal. Model.* **4** (2007), no. 1, 74–99.
- [25] B.T. Polyak, *Introduction to optimization*, Optimization Software, Inc., New York, 2010.
- [26] G. Rioux, C. Scarvelis, R. Choksi, T. Hoheisel, and P. Maréchal, *Blind deblurring of barcodes via kullback-leibler divergence*, *IEEE Transactions on Pattern Analysis and Machine Intelligence* **43** (2021), no. 1, 77–88.
- [27] R.T. Rockafellar and R.J.-B. Wets, *Variational analysis*, *Grundlehren der Mathematischen Wissenschaften [Fundamental Principles of Mathematical Sciences]*, vol. 317, Springer-Verlag, Berlin, 1998.

- [28] F. Santosa and M. Goh, *Bar code decoding in a camera-based scanner: Analysis and algorithm*, SIAM Journal on Imaging Sciences **15** (2022), no. 3, 1017–1040.
- [29] N.Z. Shor, *Minimization methods for non-differentiable functions*, vol. 3, Springer Science & Business Media, 2012.
- [30] X.-C. Tai and T.F. Chan, *A survey on multiple level set methods with applications for identifying piecewise constant functions*, Int. J. Numer. Anal. Model. **1** (2004), no. 1, 25–47.
- [31] Y. van Gennip, P. Athavale, J. Gilles, and R. Choksi, *A regularization approach to blind deblurring and denoising of qr barcodes*, IEEE Transactions on Image Processing **24** (2015), no. 9, 2864–2873.
- [32] P. Virtanen, R. Gommers, T . E. Oliphant, M. Haberland, T. Reddy, D. Cournapeau, E. Burovski, P. Peterson, W. Weckesser, J. Bright, S. van der Walt, M. Brett, J. Wilson, K. J. Millman, N. Mayorov, A. R. J. Nelson, E. Jones, R. Kern, E. Larson, C. J. Carey, I. Polat, Y. Feng, E. W. Moore, J. VanderPlas, D. Laxalde, J. Perktold, R. Cimrman, I. Henriksen, E. A. Quintero, C. R. Harris, A. M. Archibald, A. H. Ribeiro, F. Pedregosa, and P. van Mulbregt, *Scipy 1.0: Fundamental algorithms for scientific computing in python*, Nature Methods **17** (2020), 261–272.